Spectroscopy 26 (2011) 115–128
DOI 10.3233/SPE-2011-0519
IOS Press

Spectroscopic and physical–chemical characterization of ambazone–glutamate salt

Marieta Mureşan-Pop [a], Irina Kacsó [b], Xenia Filip [b], Emilia Vanea [a], G. Borodi [b], N. Leopold [a], I. Bratu [b,*] and S. Simon [a]

[a] *Babeş-Bolyai University, Faculty of Physics, Cluj-Napoca, România*
[b] *National Institute for R&D of Isotopic and Molecular Technologies, Cluj-Napoca, România*

Abstract. Ambazone monohydrate $C_8H_{11}N_7S \cdot H_2O$ (AMB), a well-known antimicrobial compound, was used together with Glutamic Acid $C_5H_9NO_4$ (Glu) to obtain a new solid form using the solvent-drop grinding procedure. The screening of the new solid form was best achieved by the combined use of X-ray Powder Diffraction (XRPD) and several spectroscopic techniques (Fourier Transformed Infrared Spectroscopy (FTIR), X-ray Photoelectron Spectroscopy (XPS), Raman and ^{13}C-NMR spectroscopy) together with Differential Scanning Calorimetry (DSC), Differential thermal analysis and thermogravimetry (DTA–TGA). The combination of the mentioned analytical techniques allows the compound to be assigned to an ambazone–glutamate salt which crystallizes in monoclinic system having the following lattice parameters: $a = 9.8352$, $b = 4.7014$, $c = 40.0987$ Å and $\beta = 94.505^\circ$. DSC, TGA data and the before mentioned spectroscopic techniques support the ambazone–glutamate salt formation.

Keywords: Ambazone, glutamic acid, XRPD, DTA–TGA, DSC, FTIR, XPS, Raman, NMR, ambazone–glutamate salt

1. Introduction

The most active areas of modern solid state chemistry represent the identification and characterization of different crystal forms (polymorphs, solvates, salts and co-crystals) of the same molecule. The investigation of crystal forms impacts on fundamental science because different crystal forms may display a range of different physical and chemical properties, which may affect application and utilization of the solid materials. Traditionally, the solid form selection process was limited to the free drug or pharmaceutically accepted salts. The solid form influences relevant physical–chemical parameters such as solubility, dissolution rate of the drug, chemical stability, melting point and hygroscopic parameter which can result in solids with superior properties [27,35]. In recent years, much of the research has been carried out on the preparation of pharmaceutical solid forms [6,10,24,26,28]. Usually, there are two methods by which solid forms may be prepared: solution-based crystallization and grinding. Mechanical and chemical methods, more commonly and usefully described as grinding, have been employed extensively in the preparation of solid forms [5]. The range of grinding conditions has been extended by the addition of solvents in the "solvent-drop" method [5,7] and this may represent the introduction of solution conditions on a limited scale to the grinding process. More recently, the use of so-called

* Corresponding author: I. Bratu, National Institute for R&D of Isotopic and Molecular Technologies, 400293 Cluj-Napoca, România. E-mail: ibratu@gmail.com.

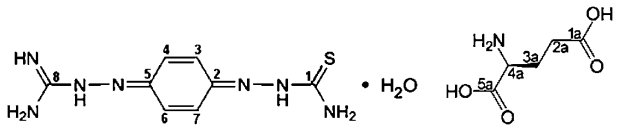

(a) (b)

Fig. 1. Chemical structures of the ambazone monohydrate (a) and of glutamic acid (b).

"solvent-drop grinding" (SDG) has been developed, in which a small quantity of a solvent is added to the solid substance or mixture prior to grinding.

Ambazone monohydrate, $C_8H_{11}N_7S \cdot H_2O$ (AMB) ([4-(2(diaminomethylidene)hydrazinyl)phenyl] iminothiourea), see Fig. 1(a), one of the oldest antimicrobial chemicals is a dark-brown, odorless, tasteless microcrystalline powder having the melting point around at 192°C up to 194°C with decomposition [22,23,25].

With a very slightly solubility in water, and in the organic solvents, it presents a bacteriostatic action on hemolytic streptococcus, streptococcus pneumonias and viridians streptococcus. The studies performed during the 1950–1960 period have shown the local antibacterial properties when it is administrated at the buccal pharyngeal cavity level, being an efficient antimicrobial drug [12]. The ulterior re-evaluation of the antibacterial AMB properties evidenced an antibacterial activity spectrum similar to that of sulfamides [21]. Recently, the antineoplasm properties of AMB were also demonstrated [1–3,11,14,18,19], that accelerated the researches on this substance, without mutagenic effects and unpleasant reactions characteristic to other oncostatic drugs [21].

Glutamic acid, $C_5H_9NO_4$ (aminopentanedioic acid) (Glu, see Fig. 1(b)) is one of the 20 proteinogenic amino acids. L-glutamic acid it is a non-essential amino acid, with the aspect as white powder that melts at 199°C with decomposition. This has physical–chemical properties and therapeutic applications in cancer therapy such as cryoprotectant, humectant, drug carrier, biological adhesive, flocculant, or heavy metal absorbent, etc. Also it takes properties as the biodegradability in the fields of food, cosmetics, medicinal and water treatments. It is use in the antitumor activity against both ovarian and breast tumors and it helps with the transportation of potassium in brain and retina [8,9,16,22,34].

As the *pKa* difference between the partners is sufficiently large [7,27], a proton transfer can take place with salt formation. AMB molecule, containing several NH and NH_2 groups with a high electron acceptor property, with $pKa = 7.39$ [22] allows the salt formation with different acids. A previous study [23] dedicated to the investigation of interaction between ambazone and hydrochloric acid (with a large *Ka*) shows the formation of a salt between these two compounds. The aim of this paper was to demonstrate by using different spectroscopic and physical–chemical methods the salt formation between glutamic acid ($pKa = 2.1$ for COOH) and the ambazone.

2. Experimental procedure

2.1. Materials and preparation

AMB was obtained from Microsin SRL Bucharest, Romania, Glu commercially available was obtained from Schuchardt OHG, Merck, Germany and these compounds were used without further purification. Solvent-drop grinding experiments were performed by placing 255.3 mg AMB with 147.13 mg Glu by addition of water in an agate mortar at room temperature, until a dried compound was obtained. The resulting sample between AMB and Glu by SDG method (AMB · Glu), were analyzed using X-ray

powder diffraction (XRPD), thermal methods (DSC, DTA–TGA) and spectroscopic techniques (FTIR, Raman, ^{13}C-NMR, XPS).

2.2. X-ray powder diffraction

XRPD patterns were obtained by using a Bruker D8 Advance diffractometer with Ge 111 monochromator in the incident beam. The experimental conditions were: the 2θ range between 3–45°, Cu Kα1 radiation ($\lambda = 1.5406$ Å) (40 kV; 40 mA), measurements were performed at room temperature. The step scan mode was performed with a step width of 0.01° at a rate of 1 step/s. The samples were mildly pre-ground in an agate mortar in order to control crystals size and to minimize the preferred orientation effects.

2.3. Thermal analysis DSC, DTA–TGA

Differential scanning calorimetry (DSC) was carried out by means of a Shimadzu DSC-60 calorimeter, the sample was heated in the range of 30–350°C with a heating rate of 10°C/min in crimped aluminum sample cell. The purge gas was a nitrogen flow of 60 ml/min. For data collection and analysis the Shimadzu TA-WS60 and TA60 2.1 software were employed.

Differential thermal analysis (DTA) and thermogravimetry (TGA) were obtained with a Simultaneous Thermogravimetric and Differential Thermal Analyzer from Shimadzu type DTG-60H. The sample was heated in the range of 30–400°C with a heating rate of 20°C/min in alumina sample cell (⌀5.8 mm × 2.5 mm) under dry nitrogen purge (70 ml/min).

2.4. FTIR spectroscopy

The FTIR spectra were recorded with a JASCO 6200 FTIR spectrometer (number of scans, 256; resolution, 4 cm^{-1}; range 4000–400 cm^{-1}). The KBr pellets were prepared by mixing 0.8 mg of sample and 150 mg KBr and pressing the mixture into a 13 mm disks at 12 tones pressure. The spectra were analyzed using Spectra Analysis software.

2.5. Raman spectroscopy

The FT-Raman instrument consisted of a Bruker FRA 106/S, EQUINOX 55 accessory attached to a FT-IR EQUINOX 55 Spectrometer and beamsplitter coating on KBr. Analysis was carried out at room temperature utilizing a laser wavelength of 1064 nm (Nd:YAG laser), power of 500 mW and an ultra-sensitive detector D 418-T Ge cooled with liquid nitrogen. Back-scattered radiation was collected at an angle of 180°. Samples were packed into an aluminium cup and a total of 32 scans were averaged for each sample at a resolution of 1 cm^{-1} in the spectral range 3600–100 cm^{-1}. The data were collected by OPUS™ Soft data acquisition software and processed by spectral analysis.

2.6. X-ray photoelectron spectroscopy (XPS)

XPS measurements were performed using a SPECS PHOIBOS 150 MCD system equipped with monochromatic AlKα source (250 W, $h\nu = 1486.6$ eV), hemispherical analyzer and multichannel detector. The typical vacuum in the analysis chamber during the measurements was in the range of 10^{-9}–10^{-10} mBar. Charge neutralization was used for all samples. The binding energy scale was charge

referenced to the C 1s at 284.6 eV. Elemental compositions were determined from spectra acquired at pass energy of 100 eV. High-resolution spectra were obtained using analyzer pass energy of 30 eV and Shirley background subtraction method was used for fitting procedure.

2.7. ^{13}C-NMR spectroscopy

Solid state cross-polarization magic-angle-spinning (CP/MAS) NMR spectra were recorded at 600 MHz ^{1}H Larmor frequency with a Bruker AVANCE III spectrometer. The SS-NMR experiment was performed on AMB, Glu and AMB · Glu solid form at room temperature. The samples were centre-packed to minimize the effect of *rf* field inhomogeneity. Standard CP/MAS experiments were performed at a spinning frequency of 10 kHz for ambazone, and 12 kHz for Glu and AMB · Glu, using a ^{1}H 90° pulse length of 3 µs. The CP/MAS NMR spectra were acquired under two-pulse phase-modulated (TPPM) ^{1}H decoupling at 100 kHz, with a recycle delay of 3 s. The CP transfer was optimized for the first Hartmann–Hahn matching condition, where the *rf* fields on the ^{1}H channel has been calibrated to 60 kHz, and the CP contact pulse was set to 1.5 ms. The ^{13}C-CP/MAS spectra of AMB, Glu and AMB · Glu solid form are calibrated according to the $^{13}CH_3$ line in TMS through an indirect procedure which uses the ^{13}C-SS-NMR resonance lines of adamantane as an intermediary standard.

3. Results and discussion

3.1. X-ray powder diffraction

X-ray powder patterns for AMB, Glu and AMB · Glu are shown in the Fig. 2. From powder pattern indexing by using Dicvol method [4] was established that AMB · Glu crystallizes in monoclinic system having following lattice parameters: $a = 9.8352$, $b = 4.7014$, $c = 40.0987$ Å and $\beta = 94.505°$. The unit cell volume is $V = 1844$ Å^3. The most probable space group obtained from systematic absences of reflections is P_{21}. The calculated density, if we consider two molecules of AMB · Glu in asymmetric unit and four molecules in the unit cell which is characteristic for this space group, is 1.39 g/cm^3. This is a reasonable value for organic compounds.

The crystallites size for the new solid form was evaluated using Scherer formula and there were obtained the following sizes: 1360 Å for AMB and 610 Å for AMB · Glu. No impurity's diffraction lines were detected by X-ray diffraction.

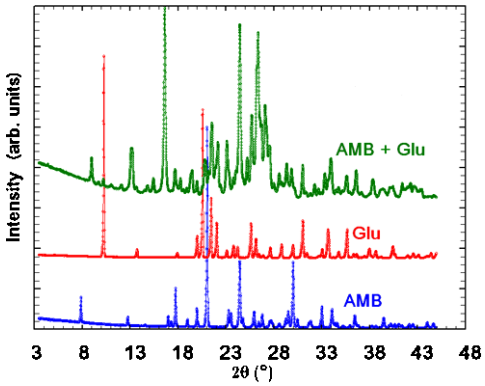

Fig. 2. XRPD for AMB, Glu and AMB · Glu. (Colors are visible in the online version of the article; http://dx.doi.org/10.3233/SPE-2011-0519.)

The powder X-ray diffraction diffractograms of the AMB, Glu and AMB · Glu are clearly different from those of the starting materials and the obtained product, confirming the presence of a new crystalline phase.

3.2. Thermal analysis DSC–DTA–TGA

The DSC thermograms of the pure AMB and of the AMB · Glu compound obtained by SDG are presented in Fig. 3. The curve for the pure AMB revealed a broad endothermic signal from 105 to 143°C, with a maximum at 125°C and $\Delta H = 36$ kJ/mol, that corresponds to the water molecules loss of the AMB monohydrate structure, followed by a sharp exothermic signal at 204.5°C, $\Delta H = 75$ kJ/mol due to the melting with decomposition of AMB. The DSC curve of AMB · Glu presents three signals: a broad endothermic peak between 75–120°C, with a maximum at 97°C and $\Delta H = 19$ kJ/mol, corresponding to the non-bonding water molecules loss, another endothermic peak between 175–185°C ($T_{\text{onset}} = 179$°C) with $\Delta H = 30$ kJ/mol due probably to the sample melting start followed by an exothermic peak with maximum at 187.8°C, $\Delta H = 106$ kJ/mol, corresponding to the decomposition of the sample.

The thermal behavior of AMB, Glu and AMB · Glu solid form obtained by SDG procedure, has been investigated by differential thermal analysis (DTA) and thermogravimetric (TGA) techniques.

The DTA–TGA curves for the pure AMB (Fig. 4) shows the 6.68% mass loss between 90–150°C and exhibits a broad endothermic peak with maximum at 133°C corresponding to the evaporation of water. In the 184–242°C temperature range significant mass loss was identified, representing 27.62% corresponding to an exothermic signal with the maximum at 215°C. In the range 242–358°C continued the decomposition of the AMB with a mass loss of ≈7.49%. These last two signals correspond to the mass loss of the volatile components resulted from the AMB decomposition.

The Glu thermal behavior (Fig. 5) in the 195–210°C temperature range shows a 10% mass loss associated with a sharp melting endotherm ($T_{\text{onset}} = 198$°C) with a maxima at 214.8°C, followed by the last mass loss of 48.26% in the range 260–370°C [20], due to the decomposition of Glu.

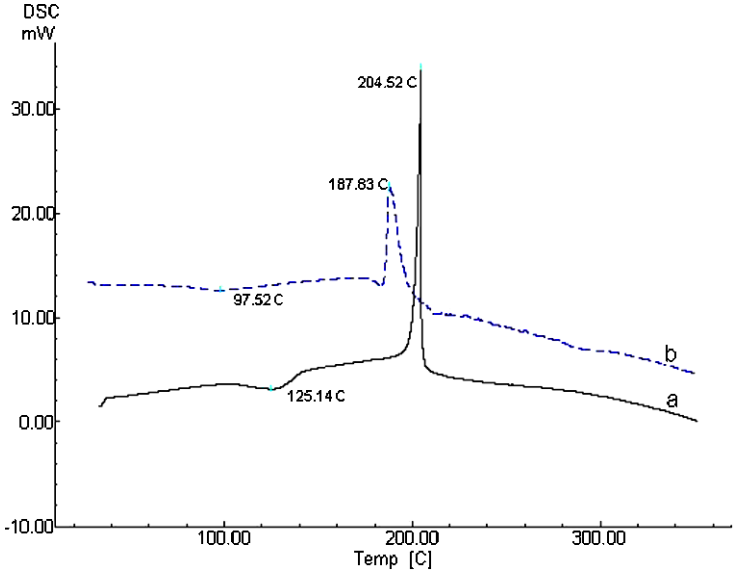

Fig. 3. DSC thermograms of AMB (a) and AMB · Glu (b). (Colors are visible in the online version of the article; http://dx.doi.org/10.3233/SPE-2011-0519.)

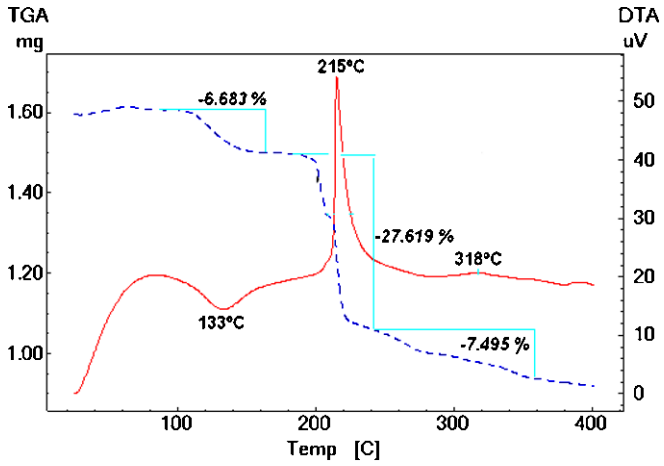

Fig. 4. DTA–TGA thermograms of AMB. (Colors are visible in the online version of the article; http://dx.doi.org/10.3233/SPE-2011-0519.)

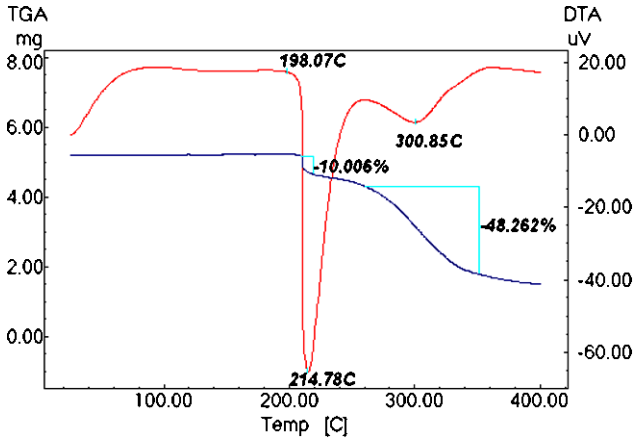

Fig. 5. DTA–TGA thermograms of Glu. (Colors are visible in the online version of the article; http://dx.doi.org/10.3233/SPE-2011-0519.)

The traces of thermal behavior of AMB · Glu (Fig. 6) shows a 5.84% mass loss between 67 and 151°C of the TGA curve, corresponding on the DTA to a broad endothermic peak with maximum at 107°C due to the water loss. In the range of 178–197°C appears a small endothermic peak ($T_{\text{onset}} = 189$°C) with maximum at 192°C corresponding to the melting start of the AMB · Glu and a 7.46% mass loss, followed by a sharp exothermic signal in the range of 197–209°C with a maximum at 204°C, when the next 9% mass loss occurs. These peaks and mass losses correspond to AMB · Glu melting followed by decomposition of the compound. The last mass loss of 24.24% in TGA appears in thermal range of 209–334°C.

DSC and TGA data are in good agreement and support the new obtained compound formation of ambazone–glutamate salt.

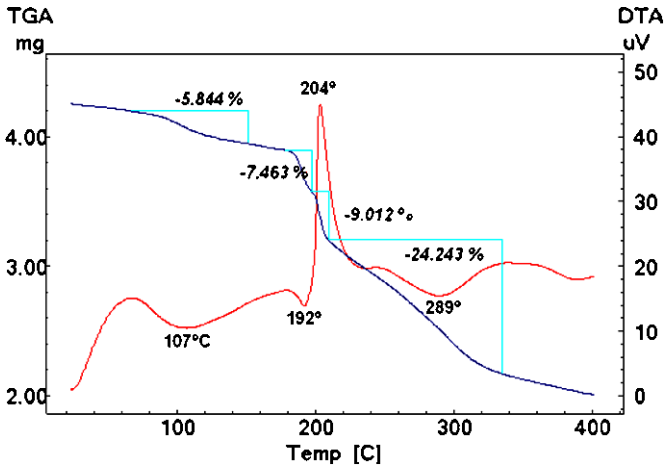

Fig. 6. DTA–TGA thermograms of AMB · Glu. (Colors are visible in the online version of the article; http://dx.doi.org/10.3233/SPE-2011-0519.)

3.3. FTIR spectroscopy

In the 3405–3395 cm^{-1} domain of the AMB spectrum, the bands observed are assigned to the NH stretching vibrations of primary amino group $–NH_2$. Figure 7 contains the stretching vibration of primary amine $–NH_2$ at ≈3397 and ≈3221 cm^{-1}. The vibration at ≈3145 cm^{-1} corresponds probably to NH secondary amine [15,23]. In the 1800–1500 cm^{-1} spectral range a medium intensity, see Fig. 8, two bands at ≈1636 and ≈1613 cm^{-1} assigned to primary amine group $–NH_2$ due to bending vibration (or C=N stretching vibration) [33] are located. The scissoring vibration of primary amine $–NH_2$ at ≈1591 cm^{-1} was also observed. In the 1580–1490 cm^{-1} range the vibration of NH secondary amine deformation vibration is identified at 1508 cm^{-1}. The bands at 1473 and 1416 cm^{-1} (medium intensity), can be assigned to aromatic C–C (in ring) stretching vibration.

In the 1230–1030 cm^{-1} range, the vibrations at 1171 and 1120 cm^{-1} (medium intensity) can be associated with C–N bending vibration. The vibration of C=S thiocarbonyl at 1151 cm^{-1} (strong intensity) was also observed.

For the new obtained compound AMB · Glu, see Fig. 7, the vibrations at ≈3426 cm^{-1} assigned to the primary amino group $–NH_2$. This fact can be explained probably by the presence of unreacted amino groups. The vibrations at 3258 cm^{-1} corresponds to the $–NH_3^+$ group, the protonated primary amine $–NH_2$, located in the range 3350–3100 cm^{-1} [15,29]. The band located at 3145 cm^{-1} in AMB is shifted to ≈3158 cm^{-1} in the AMB–GLU spectrum; it confirms the secondary amine protonation [17]. The band at ≈2930 cm^{-1} can be attributed to the $–NH_2^+$ stretching vibration [29].

The broad band at 1698 cm^{-1} (medium intensity) for AMB · Glu (see Fig. 8) can correspond to the $–NH_2^+$ deformation vibration in the solid form [15]. The secondary amine presents a band of medium intensity at 1616 cm^{-1} deformation vibration of the protonated secondary amine $–NH_2^+$.

In the 1650–1475 cm^{-1} range, the IR bands at 1601 and 1569 cm^{-1}, 1558 and 1527 cm^{-1} can be assigned to the NH_3^+ δ^{as} and $\delta^{as'}$ bending vibrations [17].

Table 1 contains the frequencies' assignments for the AMB and AMB · Glu, respectively.

Based on the vibrational frequencies' shifts and the new recorded bands one can conclude that a new solid form of AMB was formed, i.e. an ambazone–glutamate salt.

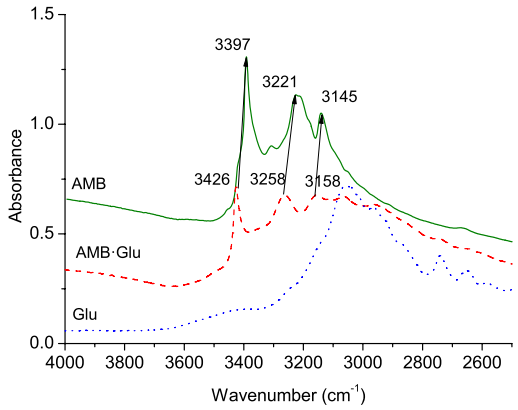

Fig. 7. FTIR spectra for AMB, AMB · Glu and Glu, spectral region 4000–2500 cm^{-1}. (Colors are visible in the online version of the article; http://dx.doi.org/10.3233/SPE-2011-0519.)

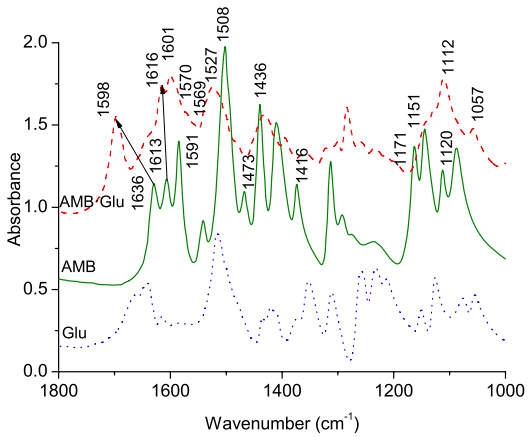

Fig. 8. FTIR spectra for AMB, AMB · Glu and Glu, spectral region 1800–1000 cm^{-1}. (Colors are visible in the online version of the article; http://dx.doi.org/10.3233/SPE-2011-0519.)

3.4. Raman spectroscopy

Raman spectra for the AMB, Glu and AMB · Glu are shown in Fig. 9 together with their vibrational frequencies' assignments. The symmetric NH_2 deformation that occurs in the region 1650–1590 cm^{-1} leads to a strong band in the IR. The primary amine group of AMB shows a band of intensity at 1600 cm^{-1} shifted to 1612 cm^{-1} (w) in the AMB · Glu spectrum [29].

In the range 1580–1490 cm^{-1} the vibration of secondary amine, NH, in the spectrum of AMB is identified at 1508 cm^{-1}. In the range 1580–1490 cm^{-1} of the AMB · Glu spectrum the vibration at 1555 cm^{-1} (w) was assigned to asymmetric $–NH_3^+$ deformation vibration. The vibration at 1527 cm^{-1} (w) is assigned to symmetric $–NH_3^+$ deformation vibration [29]. The C=S stretching vibration at 1159 cm^{-1} in the spectrum of AMB [33] is shifted to 1203 cm^{-1} in the spectrum of AMB · Glu. In the 860–680 cm^{-1} region the vibration at 776 cm^{-1} (s) is due to a strong coupling between to C=S and C=N [29] for AMB and at 786 cm^{-1} for AMB · Glu which can be a prove of the coupling diminishing.

Consequently, Raman spectroscopy demonstrates that the ambazone–glutamate structure was formed.

Table 1
The frequencies' assignments for the AMB and AMB · Glu

AMB wavenumber (cm^{-1})	AMB · Glu sdg. 1:1 wavenumber (cm^{-1})
3397 (s) and 3221 (m) NH_2-(3405–3395), w intensity, NH stretch NH_2 (s) [23]	3426 NH_2, N–H 3400–3332 (m), NH_2 3258 and 3158 (3350–3100) $–NH_3^+$ group, the protonated primary amine
3145 secondary amine	3157 secondary amine, stretch N–H [15] (m) confirms salt formation 2930-NH_2^+ stretching vibration
1636 (m) and 1613 (s) (1800–1500) NH_2 primary amine group medium intensity to bending vibration (or C=N stretching vibration) [33]	1697 asymmetric $–NH_2^+$ (m) deformation vibration 1616 deformation vibration of the protonated secondary amine $–NH_2^+$ [15]
1591, NH_2-(1640–1560) (s) NH_2 in plane band or aromatic C–C in ring (scissor vibration of primary amine $–NH_2$)	(1650–1475) the IR bands at 1601, 1569 1558 and 1527 could be assigned to the asymmetric and symmetric NH_3^+ bending vibrations [17]
1508 (1580–1490) vibration of NH secondary amine deformation vibration 1474 and 1416 aromatic C–C in ring	1482 and 1436 aromatic C–C in ring, (m), stretch
1171 and 1120 (1230–1030) (m), C–N stretch 1151 C=S thiocarbonyl (s)	1112, 1170 and 1057 NH_2-(1230–1030) (m), C–N stretch

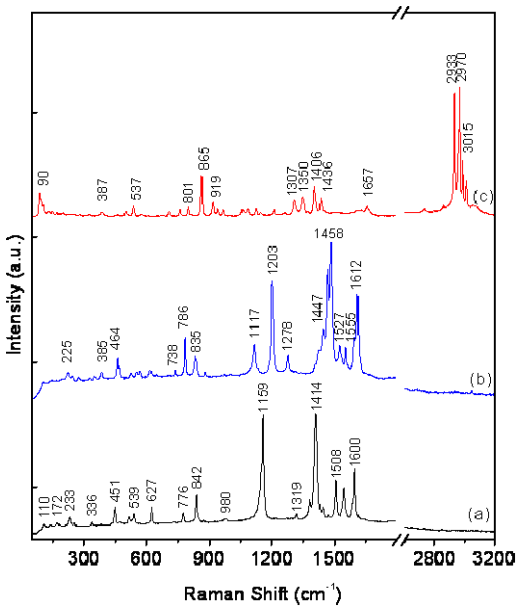

Fig. 9. Raman spectra for AMB (a), AMB · Glu (b) and Glu (c), spectral region 100–3200 cm^{-1}. (Colors are visible in the online version of the article; http://dx.doi.org/10.3233/SPE-2011-0519.)

3.5. XPS spectroscopy

XPS survey spectra evidence photoemission peaks corresponding to carbon (C 1s), nitrogen (N 1s), oxygen (O 1s) and sulphur (S 2p) photoelectrons for AMB and AMB · Glu and their KLL Auger peaks (Fig. 10). The elemental composition was determined from the survey spectra and shows a decrease in N

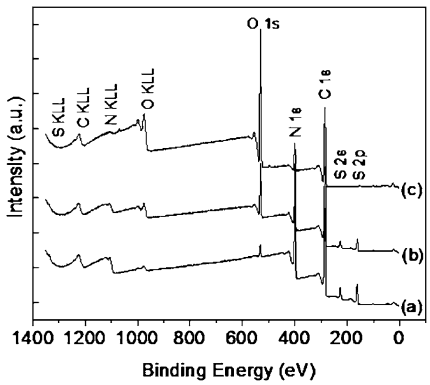

Fig. 10. Survey XPS spectra for the AMB (a), AMB · Glu (b) and Glu (c).

Table 2
Relative percentage of the main components for AMB, AMB · Glu and Glu

Sample	Elemental composition (at %)				
	C	N	C/N	S	O
AMB	58.05	31.93	1.82	6.84	3.17
AMB · Glu	59.23	23.64	2.50	4.77	12.35
Glu	60.08	9.16	6.55	–	30.75

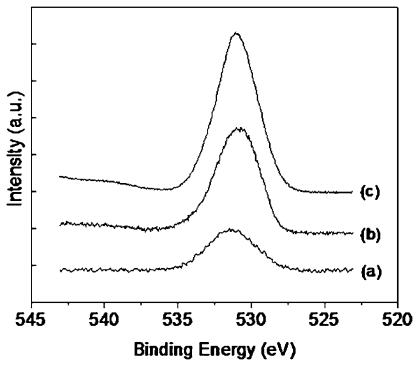

Fig. 11. O 1s high-resolution XPS spectra for the AMB (a), AMB · Glu (b) and Glu (c).

and S concentration and an increase in O and C concentration for AMB · Glu by comparison with AMB due to Glu contribution (Table 2).

With respect to the evolution of O 1s core level spectra (Fig. 11) one remarks symmetric peak for AMB due to the oxygen atom present in its structure and –OH groups adsorbed on surface from atmospheric moisture. The O 1s spectrum intensity of the complex increases and shifts to lower binding energies relative to the carboxylic emissions O=C–OH of the Glu.

The AMB C 1s core level spectrum (Fig. 12) reveals three types of carbon environment at 287.05 eV (N–C–N/N=C–NH), 284.6 eV (C=C, C–N) and 283 eV from hydrocarbon contamination [32].

Photoemissions from C 1s core level of Glu is more complex and reveals four peaks. The peak at higher binding energy (288 eV) corresponds to carbons with decreased electron density, the two carboxylic acids (COOH) [32], the peak at 285.7 eV may be assigned to C–N, the one at 284.4 eV corresponds to C

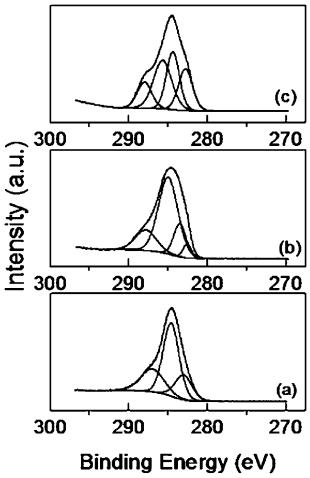

Fig. 12. Deconvoluted C 1s high-resolution XPS spectra recorded for the AMB (a), AMB · Glu (b) and Glu (c).

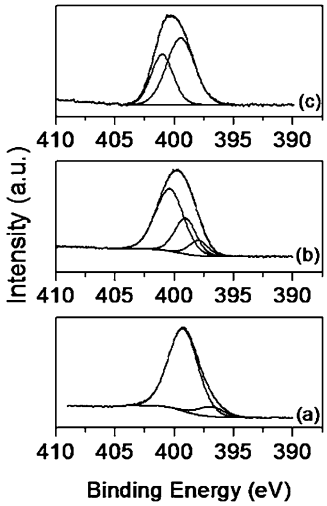

Fig. 13. Deconvoluted N 1s high-resolution XPS spectra recorded for the AMB (a), AMB · Glu (b) and Glu (c).

atoms adjacent to the carboxylic acid (C–COOH) and the peak at lowest binding energy 282.7 eV arise from hydrocarbon also present by contamination.

The AMB · Glu C 1s core level spectrum shows an increased FWHM value of 4.14 eV compared to 3.18 eV of AMB, with photoemission environment from both AMB and Glu. The slightly shift of the deconvoluted peaks from 287.05 and 284.6 eV for AMB to 287.9 and 285.03 eV, respectively, for AMB · Glu can be due to $C–NH_3^+/C{=}NH_2^+$ protonation [33].

The N 1s spectrum of AMB shows two components (Fig. 13). The component at lower binding energy (397 eV) arises from C=N photoemissions and the other one at 399.2 eV arises from the C–N nitrogen environment [31].

The deconvolution of N 1s core level spectrum of Glu reveals two components, centred at 399.4 and 401 eV, characteristic of $C–NH_2$ groups.

The nitrogen contribution in AMB · Glu N 1s core level spectrum at 400.4 eV can be ascribed to positively charged nitrogen. The formation of ambazone–glutamate salt changes the nitrogen environment reducing the electron density around N and increases the energy required to eject the electron. The shift in peak position confirms the ambazone–glutamate salt formation [13].

3.6. ^{13}C-NMR spectroscopy

The ^{13}C CP/MAS spectra of the AMB, Glu, and AMB · Glu are shown in the Fig. 14. The NMR spectra of AMB and Glu consist of eight, respectively five resonance lines, corresponding to the carbon sites in the molecular structure of these two compounds.

The chemical shifts of the resonance lines are illustrated in Table 3. A partial assignment was performed taking into account the relative intensities of the NMR lines, and also a quantum chemical computation of the ^{13}C chemical shifts in the isolated AMB molecule. On the one hand this procedure enables one to distinguish between the protonated vs. non-protonated ring carbons, and also between the C1 and C8 chemical sites. Regarding the Glu molecule, a full assignment was possible taking as a reference the ^{13}C liquid-state NMR spectrum [30]. By combining the assignments of AMB and Glu, an identification of ^{13}C CP/MAS NMR lines of AMB · Glu solid form was possible, as presented in Table 1.

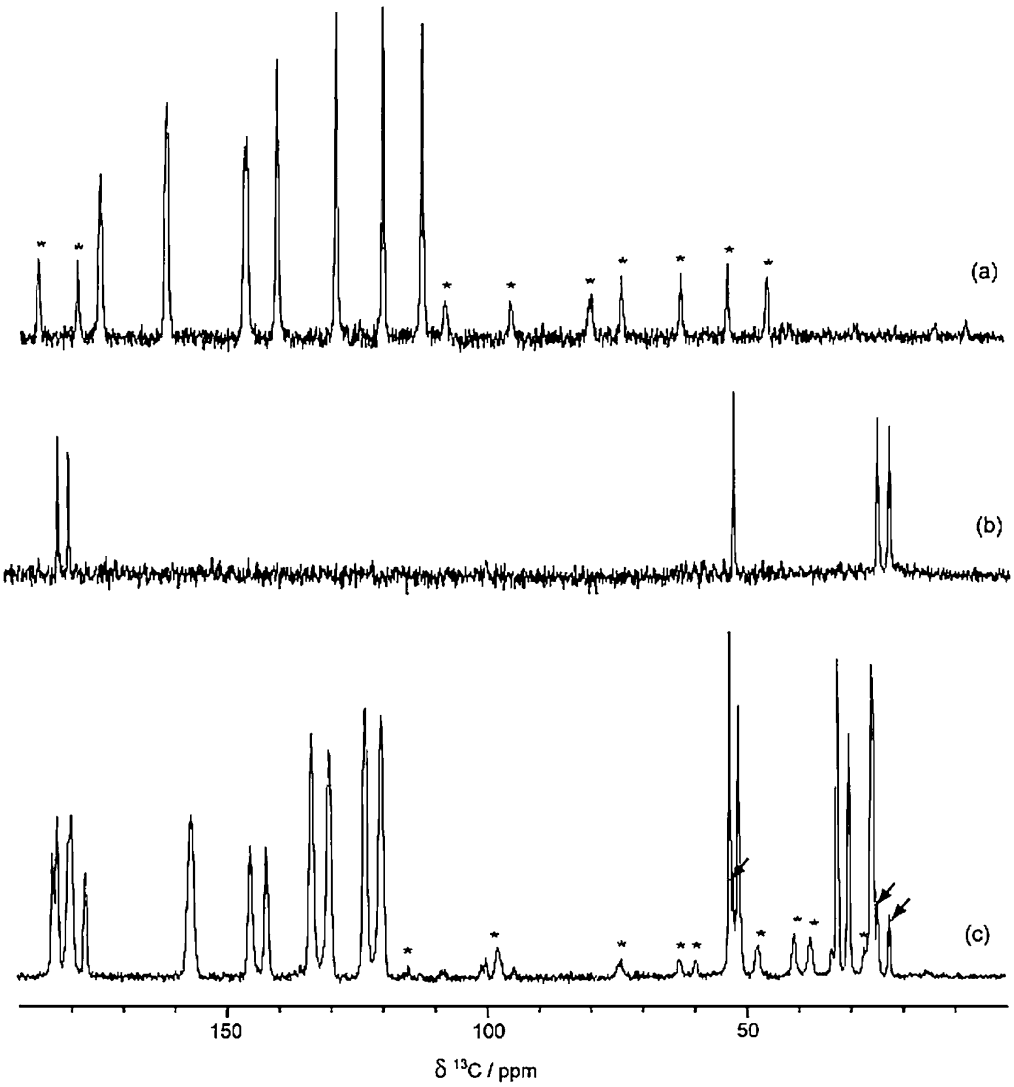

Fig. 14. The ^{1}3C CP/MAS NMR spectra of AMB (a), Glu (b) and AMB · Glu (c). The asterisks indicate spinning sidebands, and the black arrows correspond to the NMR lines of non-reacted Glu.

Analyzing the resonance lines, one can conclude that (i) there are two conformationally non-equivalent Glu molecules in the asymmetric unit of the AMB · Glu solid form and (ii) the line at 180.1 ppm (and 181.0 ppm, respectively) indicates the presence of COO^{-} site, which proves that AMB · Glu belongs to the salts class. The presence of a small quantity of Glu which remains after the chemical reaction with AMB is indicated by black arrows.

4. Conclusions

Applying the SDG method to the 1:1 ambazone:glutamic acid mixture, a compound with different physical–chemical properties was obtained. This AMB · Glu compound crystallizes in the monoclinic

Table 3
^{13}C CP/MAS NMR chemical shifts

	AMB chemical shifts (ppm)	Glu chemical shifts (ppm)	AMB · Glu chemical shifts (ppm)
Protonated aromatic carbons	112.9	–	120.1
(C3, C4, C6, C7)	120.5	–	123.1
	129.5	–	129.7
	140.9	–	133
		–	
		–	
		–	
		–	
Non-protonated aromatic carbons	146.7		141.4
(C2, C5)	147.1		144.3
C8	162.1		155.2
C1	174.8		174.9
C1a	–	25.6	28.9; 29.2
C2a	–	27.7	33.4; 35.5
C3a	–	54.4	53.8; 55.5
C4a	–	177.8	177.5; 178.1
C5a	–	178.8	180.1; 181.0

system and belongs to the $P2_1$ space group. Based on DSC–DTA–TGA measurements different thermal behaviour as compared to the initial compounds was founded. FTIR, Raman and XPS spectroscopic data show the protonation of both primary and secondary amino groups. NMR analysis evidenced the existence of the COO^- groups instead of COOH groups of the glutamic acid. These spectroscopic data demonstrate the ambazone–glutamate salt formation. Based on XRPD and NMR data we can conclude that there are two AMB · Glu molecular systems in asymmetric unit.

Acknowledgements

Investing in people! PhD scholarship, Project co-financed by the Sectoral Operational Programme Human Resources Development 2007–2013 Priority Axis 1 "Education and training in support for growth and development of a knowledge based society" Key area of intervention 1.5: Doctoral and post-doctoral programmes in support of research. Project POSDRU 6/1.5/S/3 – "Doctoral Studies: Through Science Towards Society" Babeş-Bolyai University, Cluj-Napoca, Romania. The investigations were supported by the PN 09-44 02 01/2009 and PN 09-44 02 05/2009 projects.

References

[1] R. Amlacher, J. Baumgart, A. Hartl, H. Weber, H.J. Kuhnel, W. Schulze and H. Hoffmann, *Arch. Geschwulstforsch.* **60** (1990), 11–18.
[2] R. Amlacher, A. Mackowiak, J. Baumgart, W. Schulze and H. Hoffmann, *Pharmazie* **45** (1990), 379–380.
[3] J. Baumgart, N.V. Zhukovskaya and V.N. Anisimov, *Exp. Pathol.* **33** (1988), 239–248.

[4] A. Boultif and D. Louër, *J. Appl. Cryst.* **37** (2004), 724–731.
[5] D. Braga, S.L. Giaffreda, M. Curzi, L. Maini, M. Polito and F. Grepioni, *J. Therm. Anal. Calorim.* **90** (2007), 115–123.
[6] D. Braga, F. Grepioni, L. Maini and M. Polito, *Struct. Bond.* **132** (2009), 25–50.
[7] H.G. Brittain, *Polymorphism in Pharmaceutical Solids*, Drugs and the Pharmaceutical Sciences, Vol. 192, 2nd edn, Informa Healthcare, New York, NY, 2009.
[8] L. Chun, *Adv. Drug Deliv. Rev.* **54** (2002), 695–713.
[9] L. Chun, E.J. Price, L. Milas, N.R. Hunter, S. Ke, Y. Dong-Fang and C. Charnsangavej, *Clin. Cancer Res.* **5** (1999), 891–889.
[10] M.C. Etter, SM. Reutzel and C.G. Choo, *J. Am. Chem. Soc.* **115** (1993), 4411–4412.
[11] I. Fichtner and W. Arnold, *Pharmazie* **38** (1983), 130–131.
[12] I. Fulga, *Pharmakon* **56** (2006), available at: www.pharmakon.ro/inc/arhiva/2006_02/Ambazona.pdf.
[13] S. Golczak, A. Kanciurzewska, M. Fahlman, K. Langer and J.J. Langer, *Solid State Ionics* **179** (2008), 2234–2239.
[14] W. Gutsche, A. Hartl, J. Baumgart and W. Schulze, *Pharmazie* **45** (1990), 55–57.
[15] R.A. Heacock and L. Marion, *Can. J. Chem.* **34** (1956), 1782–1795.
[16] S. Ing-Lung and V. Yi-Tsong, *Bioresource Technol.* **79** (2001), 207–225.
[17] B. Ivanova and M. Spiteller, *Spectrochim. Acta A* **77** (2010), 849–855.
[18] H.J. Kuhnel, R. Amlacher, J. Baumgart and W. Schulze, *Arch. Geschwulstforsch.* **58** (1988), 217–222.
[19] H.J. Kuhnel, R. Amlacher, K. Kramarczyk and W. Schulze, *Pharmazie* **43** (1988), 197–199.
[20] G. Liptay, *Atlas of Thermoanalytical Curves*, Akademiai Kiado, Budapest, 1973.
[21] G. Lober, K. Geller, H. Hanschmann, L.M. Popa, R. Repanovici, R. Iliescu, W. Romer, B. Janke and V. Kleinwachter, *Physiologie* **26** (1989), 305–316.
[22] G. Löber and H.Hoffmann, *Biophys. Chem.* **35** (1990), 287–300.
[23] M. Muresan-Pop, I. Kacsó, C. Tripon, Z. Moldovan, Gh. Borodi, S. Simon and I. Bratu, *J. Therm. Anal. Calorim.* **104** (2011), 299–306.
[24] M. Otsuka, K. Otsuka and N. Kaneniwa, *Drug Dev. Ind. Pharm.* **20** (1994), 1649–1660.
[25] S. Petersen, W. Gauss and E. Urbschat, *Angew. Chem.* **67** (1955), 217–231.
[26] J. Pirttimaki, E. Laine, J. Ketolainen and P. Paronen, *Int. J. Pharm.* **95** (1993), 93–99.
[27] B.S. Sekhon, *Ars Pharm.* **50** (2009), 99–117.
[28] N. Shan, F. Toda and W. Jones, *Chem. Commun. (Cambridge)* **20** (2002), 2372–2373.
[29] G. Socrates, *Infrared and Raman Characteristic Group Frequencies: Tables and Charts*, Vol. 332, 3rd edn, Wiley, West Sussex, 2001.
[30] Spectral Database for Organic Compounds SDBS, SDBS No. 1097, available at: http://riodb01.ibase.aist.go.jp.
[31] J.S. Stevens, S.J. Byard and S.L.M. Schroeder, *Crystal Growth Design* **10** (2010), 1435–1442.
[32] J.S. Stevens, J. Stephen, S.J. Byard, E. Zlotnikov, L. Sven and M. Schroeder, *J. Pharm. Sci.* **99** (2010), 4453–4457.
[33] V. Stilinovic, D. Cincik and B. Kaitner, *Acta Chim.* **55** (2008), 874–879.
[34] C. Terner, L.V. Eggleston and H.A. Krebs, Medical research council unit for research in cell metabolism, Department of Biochemistry, University of Sheffield, 1950.
[35] P. Vishweshwar, J.A. McMahon, J.A. Bis and M.J. Zaworotko, *J. Pharm. Sci.* **95** (2006), 499–516.